Critical behaviour of an interacting surface reaction model

1993 J. Phys. A: Math. Gen. 26 4197

(http://iopscience.iop.org/0305-4470/26/17/027)

J. Phys. A: Math. Gen. 26 (1993) 4197–4213. Printed in the UK

Critical behaviour of an interacting surface reaction model

Jun Zhuo†, Sidney Redner† and Hyunggyu Park‡

† Center for Polymer Studies and Department of Physics, Boston University, Boston, MA 02215, USA

‡ Department of Physics, Inha University, Inchon, 402-751, Korea

Received 19 October 1992, in final form 17 February 1993

Abstract. We investigate the kinetics of a generalized monomer–monomer surface reaction model in which there is a variable excluded-volume interaction between same species particles (*A*s and *B*s). For no interaction, this system reduces to the monomer–monomer model for which there is a first-order transition between *A*- and *B*-saturated phases. As a function of the excluded volume interaction, the first-order transition line for weak interaction terminates at a tricritical point where two second-order transitions meet. These transitions, which appear to be in the Reggeon field theory universality class, separate the *A*-saturated, reactive, and *B*-saturated phases. Series expansions and various time-dependent Monte Carlo simulations are used to estimate the critical parameters and exponents associated with these transitions.

1. Introduction

Recent investigations of idealized lattice models of surface reactions [1–4] have helped elucidate basic aspects of non-equilibrium phase transitions and have provided some insights into realistic catalytic processes [5–8]. Although only some of the basic steps in realistic catalytic reactions are accounted for in these models, their study has provided useful information about basic processes such as the oxidation of CO on metal surfaces. A common feature of these models, such as the monomer–monomer and monomer–dimer models, is that interactions between adsorbates are ignored, except for the actual surface reaction that converts the reactants into the product. When adsorbate interactions are incorporated, interesting kinetic features can result, ranging from oscillatory behaviour [9] to more complex phase behaviour [10]. However, there has not yet been a systematic effort to explore the role of interactions within the framework of the simplest stoichiometric models.

In this article, we investigate the influence of nearest-neighbour excluded-volume interactions between same species reactants on the kinetics of the monomer–monomer model. This may be viewed as each of the reactants having a radius which can be varied to be less than, or larger than the distance between adsorption sites on the surface. As we shall see, this interaction profoundly affects the non-equilibrium phase behaviour of the model. In a different context, this type of excluded-volume interaction plays a crucial role in governing the physical properties of noble gas adsorption on simple substrates, such as graphite [11]. As a function of the adsorbate radius, different types of surface ordering occur as the system is cooled to a low

0305-4470/93/174197+17 $07.50

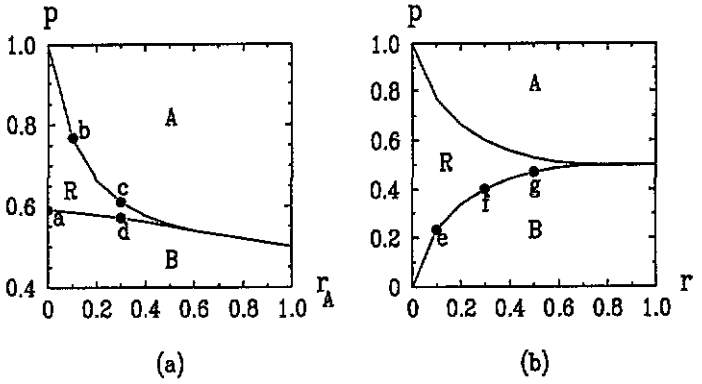

Figure 1. The phase diagrams of the interacting surface reaction model for (a) r_A variable and $r_B = 1$, and (b) $r_A = r_B = r$. Here R refers to the reactive phase, while A and B refer to the two respective saturated phases where the surface is filled by one species and no further reaction is possible. Time-dependent MC simulations were performed at the points marked by lower-case letters.

temperature. Certain aspects of this ordering underlie the different phase transitions that occur in our interacting reaction model.

Another motivation for studying surface reactions with adsorbate interactions stems from the interesting behaviour exhibited by the recently-introduced 'dollars and dimes' model [12]. This a monomer–monomer model in which one of the species (the 'dollar') has a diameter greater than a lattice spacing, so that nearest-neighbour adsorbed dollars cannot occur. This system corresponds to the limiting case of infinitely strong excluded volume in our general interacting model. The dollars and dimes model exhibits a second-order transition between a dime-saturated phase and a reactive steady state which is in the Reggeon field theory (RFT) universality class. On the other hand, when the interaction strength goes to zero, the reaction reduces to the simple monomer–monomer model [13], for which there is a first-order transition between an a A-saturated and a B-saturated state as the relative deposition rates of the two species passes through unity. We are interested in determining how the general interacting model interpolates between these two limiting behaviours as the interaction strength is varied.

As the strength of the excluded–volume interaction increases, the transition of the monomer–monomer model appears to extend to a first-order line which separates A- and B-saturated states. At a critical value of the interaction, the first-order transition terminates at a tricritical point beyond which there are two second-order transitions (figure 1). The lower transition separates the B-saturated and reactive steady states, while the upper transition separates the A-saturated and steady states. In the limit of infinitely strong exluded-volume interaction between As, nearest-neighbour pairs cannot occur, and the A-saturated phase does not exist. Thus there is only a single transition in this limit. We have employed the complementary numerical techniques of series expansions and Monte Carlo simulations to map out the phase diagram and determine the nature of the associated non-equilibrium phase transitions.

In section 2, we first define our interacting surface reaction model. The results of a single-site mean-field approximation are outlined in section 3, where a tricritical point is predicted to occur only in the monomer–monomer limit. In section 4, we review the scaling behaviour of basic time-dependent properties in surface reaction phenomena.

Series expansions of these surface properties and the corresponding analysis are presented in section 5. Complementary Monte Carlo simulation results are given in section 6. Both of these numerical methods suggest the phase diagram of figure 1, with a tricritical point at a finite value of the excluded-volume interaction.

2. The model

We generalize the monomer–monomer model to allow for a nearest-neigbour repulsion between same species particles (the As, for example). This is parameterized by specifying that an A can adsorb adjacent to an already-adsorbed A (restricted vacancy) at a rate $r_A k_A$, with $0 \leqslant r_A \leqslant 1$, where k_A is the 'bare' adsorption rate of the As. Thus the limiting case $r_A = 0$ corresponds to the dollar and dime model in which nearest-neighbour adsorbed As cannot exist, while the case $r_A = 1$ corresponds to the monomer–monomer model. These steps can be schematically summarized as:

$$A + S' \xrightarrow{k_A} A_s$$

$$A + S'' \xrightarrow{r_A k_A} A_s$$

$$B + S \xrightarrow{k_B} B_s$$

$$A_s + B_s \xrightarrow{k_r} (AB) \uparrow + 2S.$$

Here the subscript s denotes adsorbed particles, S denotes a vacant lattice site, and S' or S'' denotes an unrestricted or restricted vacant lattice site for the As. The restricted vacancies S'' have at least one A_s in their nearest-neighbourhood. Here we will consider only the adsorption-limited reaction, where the reaction rate is much greater than the adsorption rates, $k_r \gg k_A, k_B$. The phase diagram of this model is sketched in figure 1.

To formulate a convergent series expansion (section 5), it is necessary to introduce a small modification to the excluded–volume interaction described above. This alteration does not affect the nature of the reaction in any substantial way, but it does render the supercritical series expansion convergent. Whenever there is an A adsorption attempt at a vacant site which neigbours both an A_s and a B_s, we ignore the excluded–volume interaction, and allow the A to adsorb and react immmediately with the B_s, thus forming an AB product. This change is equivalent to a small increase in the excluded–volume parameter r_A (when r_A is strictly in the range $0 < r_A < 1$), an attribute which should not affect the overall phase diagram of the system.

This interacting surface reaction model can also be generalized to allow for excluded-volume interactions for both species. For example, we may define an excluded-volume parameter for both A and B adsorption, r_A and r_B, respectively. In particular, when the magnitude of the interaction for each species is the same, the phase diagram is symmetric about equal adsorption rates for the two species (figure 1(b)), a feature which simplifies analysis of the model.

3. Mean-field theory

To gain a first impression for the kinetics of the interacting surface reaction model, we

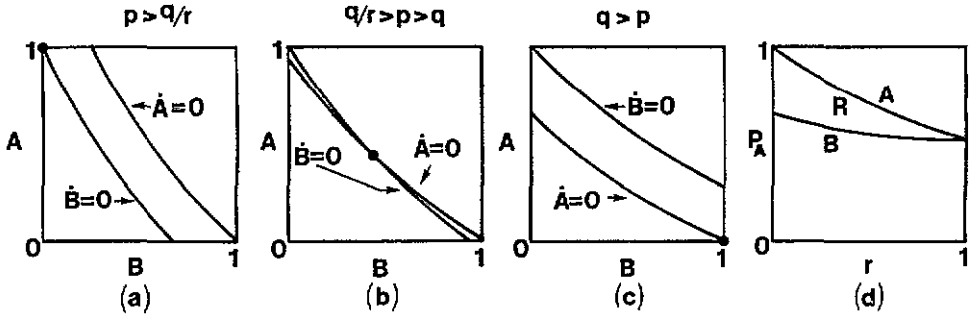

Figure 2. Schematic plot of the nullclines $\dot{A}=0$ and $\dot{B}=0$ from the single-site mean-field theory (equation (2)). Shown are the nullclines for (a) $p>q/r$, (b) $q/r>p>q$, and (c) $q>p$. The resulting stable fixed points for these three cases are marked by the dot. This fixed-point behaviour leads to the phase diagram shown in (d). Note that the width of the steady-state region vanishes linearly in $1-r$ as $r\to 0$.

outline the results from a single-site mean-field analysis. For concreteness, we consider the situation where $r_B=1$, and also denote r_A as r in this section. On a lattice of coordination number z, the concentration of As and Bs evolve according to

$$\dot{A}=E[p(E^z+r((E+A)^z-E^z))-q(1-(1-A)^z)]$$
$$\dot{B}=E[q(1-A)^z-p(1-(1-B)^z)]. \tag{1}$$

Here A and B also refer to the concentration of the two species, $E=1-A-B$ is the concentration of vacant sites, $p=k_A/(k_A+k_B)$ is the probability that an A adsorption attempt occurs, and $q=1-p$ is the probability of a B adsorption attempt.

In the equation for $\dot{A}$, the first term accounts for the probability that an A adsorbs onto a site with no nearest-neighbour Bs. This term is further separated into the contribution due to A adsorption on a vacanacy with the nearest-neighbourhood also vacant, and a contribution where the nearest-neighbourhood contains As but no Bs. The second term gives the probability of B adsorption onto a site in which there is at least one A in the nearest neighbourhood. In the equation for $\dot{B}$, the second term which accounts for A adsorption, does not involve the factor r, since it is explicit that there is at least one B in the nearest neighbourhood.

To determine the phase diagram, we analyse the nullclines $\dot{A}=0$ and $\dot{B}=0$, given by

$$pry_B^z+p(1-r)E^z-q(1-y_A)^z=0 \qquad qy_A^z-p(1-y_B^z)=0 \tag{2}$$

where $y_A=1-A$ and $y_B=1-B$. Graphs of the nullclines as a function of A and B are shown in figure 2. As p varies, there is a continuous evolution for the location of the stable fixed point. This corresponds to a second-order transition from an A saturated phase when $p>q/r$, to a reactive steady state for $q/r>p>q$, and finally to a B saturated phase for $q>p$. According to this mean-field analysis, the transition point in the monomer–monomer model is actually a tricritical point where the A- and B-saturated phases and the reactive phase meet. The width of the steady-state regime vanishes linearly in $1-r$, as $r\to 1$. Indeed, given the known behaviour at the two endpoints $r=0$ and $r=1$, the mean-field form of the phase diagram is the most natural outcome from polynomial rate equations. Thus one of the goals of our numerical study will be to determine the validity of the mean-field predictions and the quantitative properties of the various non-equilibrium phase transitions.

4. Scaling behaviour

Our numerical studies are based on examining the time dependence of several basic geometric properties of the reactive surface, when the lattice is initially filled by one species, except for a single vacancy. Here we illustrate the case where Bs occupy the system. Following closely Grassberger and de la Torre [14], we hypothesize that any function of x, t, and $\Delta = p - p_c$ exhibits power law dependences on these quantities multiplied by a function which depends only on the scaling variables x^2/t^z and $\Delta t^{1/\nu}$. Here p_c is critical value of p, and ν and z are critical exponents.

For the density of vacancies at position x, one expects

$$\rho(x, t) \sim t^{m-dz/z} F(x^2/t^z, \Delta t^{1/\nu}) \tag{3}$$

and for the survival probability—the probability that the system has not yet entered into the B-saturated state at time t—one expects

$$P(t) \sim t^{-\delta} \phi(\Delta t^{1/\nu}) \tag{4}$$

where δ and η are additional critical exponents, while F and ϕ are universal scaling functions.

From (3), the average number of vacancies, $N_E(t)$, and the mean-square spread of the region of vacancies, $R^2(t)$, are given by

$$N_E(t) = \int d^d x \rho(x, t) \sim t^{\eta} f(\Delta t^{1/\nu}) \tag{5}$$

and

$$R^2(t) = \frac{1}{N_E(t)} \int d^d x x^2 \rho(x, t) \sim t^z g(\Delta t^{1/\nu}). \tag{6}$$

In the supercritical region where $\Delta > 0$, the system has non-zero chance of survival (i.e. not becoming saturated by Bs) in the long-time limit. Therefore

$$P_\infty \equiv \lim_{t \to \infty} P(t) \sim \Delta^{\nu\delta}. \tag{7}$$

In the subcritical region where $\Delta < 0$, one expects the survival probability and the average number of vacant sites to decay exponentially in time

$$P(t) \sim t^{\alpha_1} \exp(-\text{constant} \times t), \tag{8}$$

$$N_E(t) \sim t^{\alpha_2} \exp(-\text{constant} \times t) \tag{9}$$

where α_1 and α_2 are unknown exponents. These formulae can be true only if the scaling functions in (3) and (4) satisfy

$$\phi(y) \sim (y)^{\alpha_1 + \nu\delta} e^{-b(-y)^{\nu}} \qquad \text{for } y \to \infty \tag{10}$$

$$f(y) \sim (-y)^{\alpha_2 - \nu\eta} e^{-c(-y)^{\nu}} \qquad \text{for } y \to \infty \tag{11}$$

where b and c are constants. Inserting (10), (11) into (5), (6), respectively, taking the Laplace transform and letting $s \to 0$, we find

$$\tilde{P}(0) \sim (-\Delta)^{-\nu(1-\delta)} \tag{12}$$

and

$$\tilde{N}_E(0) \sim (-\Delta)^{-\nu(1+\eta)} \tag{13}$$

where the tilde denotes the Laplace transform. Equations (7), (12) and (13) are the quantities which will be computed by series expansions in the next section to provide estimates for critical exponents.

5. Series expansions

Recently, Dickman and Jensen developed a time-dependent perturbation theory for two-state interacting particle systems which exhibit a non-equilibrium continuous phase transition to a unique absorbing state [15, 16]. They presented several methods for deriving series expansions for the evolution of a state with a single seed particle, including expansions for the ultimate survival probability of the seed in both the super- and subcritical regions, the average number particles in the subcritical regions, as well as short time expansions. Here, their theory is adapted to our interacting surface reaction model in one dimension.

We begin by briefly reviewing the theory for the series expansion in the context of our model. Since each site can exist in three states, the basis states for given site $i \in \mathfrak{L}^d$ are $|\sigma_i\rangle$ with $\sigma_i = 0, 1$ or 2, corresponding to site i being occupied by a B, vacant, or occupied by an A, respectively. An arbitrary configuration of the system, $|\{\sigma_i\}\rangle$, can be written as a direct product $|\{\sigma_i\}\rangle \equiv \Pi_{i \in \mathfrak{L}^d} |\sigma_i\rangle$. Thus the state of the system at time t is

$$|\Psi(t)\rangle = \sum_{\{\sigma_i\}} p(\{\sigma_i\}, t)|\{\sigma_i\}\rangle \tag{14}$$

where the sum is over all configurations, and $p(\{\sigma_i\}, t)$ is the configuration probability distribution. The evolution of a state is governed by the master equation

$$\frac{\partial|\Psi(t)\rangle}{\partial t} = \mathcal{H}|\Psi(t)\rangle \tag{15}$$

where $\mathcal{H}$ is the time evolution operator. The formal solution to this equation is,

$$|\Psi(t)\rangle = \mathrm{e}^{\mathcal{H}t}|\Psi(0)\rangle \tag{16}$$

where $|\Psi(0)\rangle$ is the initial state.

The time evolution operator $\mathcal{H}$ for our interacting model can be written as

$$\mathcal{H} = p\mathcal{D}_A + q\mathcal{D}_B, \tag{17}$$

where $\mathcal{D}_A$ and $\mathcal{D}_B$ are the operators that describe the deposition and subsequent possible reaction of A and B particles, respectively. To compute the action of $\mathcal{H}$, consider a configuration $|\gamma\rangle$ which contains n_E vacancies and m restricted vacancies (where at least one of its nearest neighbours is occupied by an A and none of its neighbours is occupied by a B). Then the action of $\mathcal{D}_A$ on $|\gamma\rangle$ yields

$$\mathcal{D}_A|\gamma\rangle = \sum_{i=1}^{n_E - m} |\gamma_i'\rangle + r_A \sum_{i=1}^{m} |\gamma_i''\rangle - [n_E + (r_A - 1)m]|\gamma\rangle \tag{18}$$

where $|\gamma'\rangle$ or $|\gamma''\rangle$ are the configurations generated from $|\gamma\rangle$ by depositing an A on one of the unrestricted or restriced vacant sites of $|\gamma\rangle$, respectively, and then allowing a reaction to occur with a neighbouring B if one exists. The action of $\mathcal{D}_B$ on a

configuration is defined similarly. Performing the Laplace transform of (16) and inserting (17) yields:

$$|\tilde{\Psi}(s)\rangle = \int_0^\infty e^{-st}|\Psi(t)\rangle\, dt = (s - p\mathcal{D}_A - q\mathcal{D}_B)^{-1}|\Psi(0)\rangle. \tag{19}$$

There are two ways of performing a perturbation expansion of (19), by taking either q or p as the small expansion parameter, corresponding to the supercritical or subcritical expansion, respectively. We shall drive these expansions for an initial distribution which assigns probability 1 to the configuration $|X_0\rangle$ in which all lattice sites are occupied by Bs, except for a vacancy at the origin.

5.1. Supercritical expansion

Let $\lambda = q/(1-q)$ and $s' = s/(1-q)$, then except for an overall factor $(1-q)^{-1}$ (which can be accounted for at the end of the calculation), equation (19) becomes:

$$|\tilde{\Psi}(s)\rangle = (s' - \mathcal{D}_A - \lambda\mathcal{D}_B)^{-1}|\Psi(0)\rangle. \tag{20}$$

Under the assumption that $|\tilde{\Psi}(s)\rangle$ can be expanded in powers of λ

$$|\tilde{\Psi}(s)\rangle = |\tilde{\Psi}_0(s)\rangle + \lambda|\tilde{\Psi}_1(s)\rangle + \lambda^2|\tilde{\Psi}_2(s) + \cdots. \tag{21}$$

We define $O_A(s) = (s - \mathcal{D}_A)^{-1}$ and treat $\lambda\mathcal{D}_B$ perturbatively. Upon inserting (21) in (20), we thus find

$$|\tilde{\Psi}_0\rangle = O_A|X_0\rangle$$

$$|\tilde{\Psi}_n\rangle = O_A\mathcal{D}_B|\tilde{\Psi}_{n-1}\rangle \qquad n \geq 1. \tag{22}$$

As the above equations show, the operator O_A plays a fundamental role in the supercritical expansion. The effect of this operator on an arbitrary configuration $|\gamma\rangle$ can be found by using the identity

$$O_A|\gamma\rangle = s^{-1}|\gamma\rangle + s^{-1}O_A\mathcal{D}_A|\gamma\rangle. \tag{23}$$

Inserting (18) into (23) and rearranging yields

$$O_A|\gamma\rangle = [s + n_E + (r_A - 1)m]^{-1}\left[|\gamma\rangle + O_A\left(\sum_{i=1}^{n_E-m}|\gamma_i'\rangle + r_A\sum_{i=1}^{m}|\gamma_i''\rangle\right)\right]. \tag{24}$$

Suppose that configuration $|\gamma\rangle$ contains n_E vacancies and n_A As. We define the *order* of $|\gamma\rangle$ as $(n_A + 2n_E)$. This is the number of B absorptions needed to reach the saturated state from $|\gamma\rangle$. It is easy to see that each action of $\mathcal{D}_A(\mathcal{D}_B)$ on a given configuration will generate new configurations whose order will increase (decrease) by one. It is also clear from the nature of the supercritical expansion that $|\tilde{\Psi}(s)\rangle$ involves infinitely many configurations, so it cannot be computed for an infinite lattice. However, one can compute the Laplace transform of the *saturation* probability, $\tilde{p}(s)$, i.e. the probability of having entered the B-saturated state when the system started in state $|X_0\rangle$. The term of order λ^j in the expansion for $\tilde{p}(s)$ is simply the coefficient of $|0\rangle$ in $|\tilde{\Psi}_j\rangle$. As each application of $\mathcal{D}_B$ on a configuration will yield configurations whose order is lowered at most by one, it follows from (22) that in a calculation of $\tilde{p}(s)$ to $O(\lambda^n)$, we can discard all configurations with order higher than n in the expression for $|\tilde{\Psi}_0\rangle$. Similarly, we can ignore all configurations with order higher than $(n-k)$ in

$|\tilde{\Psi}_k\rangle$, as none of these contribute to the saturation probability. If we merely wish to compute the ultimate survival probability, using the identity

$$[P_\infty = 1 - \lim_{s\to 0} s\tilde{p}(s)$$

the application of (24) becomes much simpler, because the algebraic factor in front of (24) reduces to a numerical factor $1/(n_E + (r_A - 1)m]$.

To illustrate the method, we calculate the ultimate survival probability to third order. For this, we first require $|\tilde{\Psi}_0\rangle$ to third order

$$|\tilde{\Psi}_0\rangle = O_A|X_0\rangle = O_A|1\rangle = |1\rangle + \tfrac{1}{2}|11\rangle + \tfrac{1}{3}|111\rangle + \cdots$$

where higher-order configurations are discarded since they do not contribute to the survival probability at third order. Then the action of the operator for the addition of a B on $|\tilde{\Psi}_0\rangle$ gives

$$\mathfrak{D}_B|\tilde{\Psi}_0\rangle = r_B(|0\rangle - |1\rangle) + \frac{r_B}{2}2|1\rangle - (2|11\rangle) + \tfrac{1}{3}(2r_B|11\rangle + |101\rangle)$$

$$= r_B|0\rangle + \tfrac{1}{3}(|101\rangle - r_B|11\rangle)$$

which implies

$$|\tilde{\Psi}_1\rangle = O_A\mathfrak{D}_B|\tilde{\Psi}_0\rangle = \frac{r_B}{s'}|0\rangle + \tfrac{1}{6}(|101\rangle - r_B|11\rangle).$$

Similarly, using $\mathfrak{D}_B|\tilde{\Psi}_1\rangle = \frac{1}{3}r_B(1 - r_B)|1\rangle$ gives

$$|\tilde{\Psi}_2\rangle = O_A\mathfrak{D}_B|\tilde{\Psi}_1\rangle = \tfrac{1}{3}r_B(1 - r_B)|1\rangle$$

and then using $\mathfrak{D}_B|\tilde{\Psi}_2\rangle = \frac{1}{3}r_B^2(1 - r_B)|0\rangle$, yields

$$|\tilde{\Psi}_3\rangle = O_A\mathfrak{D}_B|\tilde{\Psi}_2\rangle = \frac{1}{3s'}r_B^2(1 - r_B)|0\rangle.$$

Here we have used $\mathfrak{D}_B|0\rangle = 0$. Since the coefficient of order λ^k in the series for P_∞ *equals* $(-s/p)$ *times the coefficient of* $|0\rangle$ *in* $|\tilde{\Psi}_k\rangle$ *in the* $s \to 0$ *limit, the first three terms* in the series for P_∞ are,

$$P_\infty = 1 - r_B\lambda - 0\lambda^2 - \tfrac{1}{3}r_B^2(1 - r_B)\lambda^3 + O(\lambda^4).$$

Notice that P_∞ is independent of r_A up to this order; in fact, r_A does not apear until the 5th order, when configurations such as $|1211\rangle$ or $|1121\rangle$ need to be considered. For such configurations, the application of O_A can be computed following the methods described above. For example, we find

$$O_A|1121\rangle = \frac{1}{2 + r_A}[|1121\rangle + O_A(|11121\rangle + r_A|1221\rangle + |11211\rangle)].$$

The formalism described above can be codified as a computer program to calculate series expansions for P_∞. We have thereby derived the series expansion for P_∞ to 20th

order in λ for a mesh of (r_A, r_B) values. As an example, we give the series for P_∞ for $r_A = 0.3$ and $r_B = 0.3$

$$P_\infty = 1 - 0.3\lambda - 0.021\lambda^3 - 0.0056\lambda^4 - 0.000\,920\,246\,376\,8\lambda^5 - 0.004456655424\lambda^6$$
$$+ 0.0015549375025555\lambda^7 - 0.00224779674146662\lambda^8 + 0.000645079371414\lambda^9$$
$$- 0.0007623383775736\lambda^{10} + 0.000568829584095\lambda^{11}$$
$$- 0.0011296776786072\lambda^{12}$$
$$+ 0.0013448441643274\lambda^{13} - 0.001390875415489\lambda^{14}$$
$$+ 0.000936249941273\lambda^{15}$$
$$- 0.0001880195548484\lambda^{16} - 0.000953488725215\lambda^{17}$$
$$+ 0.002441113996814\lambda^{18}$$
$$- 0.0040510934482114\lambda^{19} + 0.004987190933985\lambda^{20} + O(\lambda^{21}).$$

Substituting $\lambda = q/(1-q)$ in this equation yields a series in q.

5.2. *Subcritical expansion*

The subcritical expansion is very similar in character to the supercritical expansion, as one starts with (21)–(24). However, the roles of $\mathcal{D}_A$ and $\mathcal{D}_B$ are interchanged and λ is replaced by $\mu = \lambda^{-1}$. For the subcritical case, it is useful to define $O_B(s) = (s - \mathcal{D}_B)^{-1}$, as the operator that plays the role analogous to O_A in the supercritical expansion. There is one crucial difference between the two formalisms, however. In the supercritical expansion, the action of O_A on a non-saturated configuration generates an *infinite* number of terms. On the other hand, for the subcritical expansion, the operation of O_B on the same configuration generates only a *finite* number of terms. Therefore, we are able to calculate a wider range of quantities than in the supercritical expansion, including $\tilde{P}(0)$, $\tilde{N}_E(0)$ and $\tilde{N}_A(0)$. In particular, the coefficient of μ_Σ^j in the expansion for $\tilde{P}(0)$ is the sum of the coefficients in the expansion for $|\Psi_j\rangle$, excluding the contribution of the B-saturated state. Similarly, the corresponding coefficient in the expansion for $\tilde{N}_E(0)$ ($\tilde{N}_A(0)$) is just the sum of the product of the coefficients times the number of vacancies (As) for each configuration. We then obtain information about critical exponents through the scaling relations (12) and (13).

As an example, we calculate the subcritical expansion for $\tilde{P}(0)$ and $\tilde{N}_E(0)$ to 2nd order in μ. Applying O_B on the initial configuration yields:

$$|\tilde{\Psi}_0\rangle = O_B|X_0\rangle = O_B|1\rangle = \frac{1}{r_B}(|1\rangle + r_B O_B|0\rangle).$$

Notice that unlike the corresponding quantity in the supercritical expansion, here $|\tilde{\Psi}_0\rangle$ consists of only a finite number of terms. From (20) we get:

$$\mathcal{D}_A|\tilde{\Psi}_0\rangle = \frac{1}{r_B}(|11\rangle - |1\rangle)$$

where we have used $\mathcal{D}_A O_B|0\rangle = 0$. Continuing this expansion in the same manner as above, we obtain

$$|\tilde{\Psi}_1| = O_B \mathcal{D}_A |\tilde{\Psi}_0\rangle = \frac{1}{r_B}\left[\frac{1}{2r_B}(|11\rangle + 2r_B O_B|1\rangle) - O_B|1\rangle\right] = \frac{1}{2r_B^2}|11\rangle$$

$$\mathcal{D}_A|\tilde{\Psi}_1\rangle = \frac{1}{2r_B^2}(2|111\rangle - 2|11\rangle) = \frac{1}{r_B^2}(|111\rangle - |11\rangle)$$

$$|\tilde{\Psi}_2\rangle = O_B \mathcal{D}_A |\tilde{\Psi}_1\rangle = \frac{1}{r_B^2}\left[\frac{1}{(1+2r_B)}(|111\rangle + 2r_B|11\rangle + O_B|101\rangle) - O_B|11\rangle\right]$$

$$= \frac{1}{r_B^2(1+2r_B)}[|111\rangle + \frac{1}{2r_B}(|101\rangle - |11\rangle)].$$

Thus up to 2nd order in μ, we sum the coefficients in $|\tilde{\Psi}_j\rangle$ to obtain

$$\tilde{P}(0) = \frac{1}{r_B} + \frac{1}{2r_B^2}\mu + \frac{1}{r_B^2(1+2r_b)}\mu^2 + O(\mu^3)$$

and by forming the sum of the product of the appropriate coefficients and the number of empty sites, we obtain

$$\tilde{N}_E(0) = \frac{1}{r_B} + \frac{1}{r_B^2}\mu + \frac{3}{r_B^2(1+2r_B)}\mu^2 + O(\mu^3).$$

This procedure has also been codified into a computer program to calculate the series expansions for $\tilde{P}(0)$, $\tilde{N}_E(0)$ and $\tilde{N}_A(0)$ to 19th order in μ. We give below the series expansion for $\tilde{N}_E(0)$ at $r_A = 0.3$ and $r_B = 1$:

$$\begin{aligned}\tilde{N}_E(0) = {} & 1 + 1\mu + 1\mu^2 + 1\mu^3 + 1\mu^4 + 0.84444444444444\mu^5 + 0.815277777777778\mu^6 \\ & + 0.667013888888889\mu^7 + 0.600594997427981\mu^8 + 0.490312976358878\mu^9 \\ & + 0.4259539441433\mu^{10} + 0.343240313423238\mu^{11} + 0.288898991754849\mu^{12} \\ & + 0.23549400921303\mu^{13} + 0.191490976074571\mu^{14} \\ & + 0.155590529333808\mu^{15} \\ & + 0.12529735823576\mu^{16} + 0.10272200607331\mu^{17} \\ & + 0.0780490514121529\mu^{18} \\ & + 0.0680461675618859\mu^{19} + O(\mu^{20}).\end{aligned}$$

To obtain the corresponding series expansion in p, simply substitute $\mu = p/(1-p)$ into the series expansion and divide the resulting series by $(1-p)$.

5.3. Series analysis and results

Our computer program may be used to derive subcritical or supercritical expansions of the interacting surface reaction model for arbitrary r_A and r_B, and we focused on the two special cases of $r_B = 1$ and $0 \leqslant r_A \leqslant 1$, and $r_A = r_B$. A number of series analysis methods were attempted; empirically, we found that Padé approximants to the logarithmic derivative of the series gave the best results for the supercritical series,

Table 1. Estimates for the location of the critical points and the corresponding critical exponents of P_∞ for the interacting model with $r_B = 1$. The * indicates that defective approximants were used in determining the numerical estimate for p_c and the exponent.

r_A	Lower p_c	Lower $\delta\nu$	Upper p_c	Upper $\delta\nu$
0.0	0.5909 ± 0.0005	0.283 ± 0.005		
0.1	0.5849 ± 0.0002	0.283 ± 0.003	0.7647 ± 0.0007	0.249 ± 0.006*
0.2	0.5773 ± 0.0002	0.301 ± 0.004	0.6654 ± 0.0007	0.239 ± 0.009*
0.3	0.5684 ± 0.0002	0.338 ± 0.004	0.6101 ± 0.0004	0.251 ± 0.006*
0.4	0.5595 ± 0.0011	0.377 ± 0.024*	0.5769 ± 0.0003	0.315 ± 0.005*
0.5	0.5491 ± 0.0007	0.458 ± 0.018*	0.5545 ± 0.0002	0.408 ± 0.006*
0.6	0.5385 ± 0.0007	0.563 ± 0.015	0.5383 ± 0.0002	0.524 ± 0.006*
0.7	0.5285 ± 0.0001	0.661 ± 0.004	0.5261 ± 0.0001	0.656 ± 0.002
0.8	0.5186 ± 0.0002	0.772 ± 0.007	0.5154 ± 0.0002	0.766 ± 0.003
0.9	0.5094 ± 0.0003	0.879 ± 0.008	0.5074 ± 0.0003	0.901 ± 0.019*
1.0	0.5000 ± 0.0000	1.000 ± 0.000	0.5000 ± 0.0000	1.000 ± 0.000

and that differential approximants [17] yielded good estimates for the critical behaviour in the subcritical regime.

Shown in tables 1–4 are the results of unbiased estimates of the critical parameters for the case $r_B = 1$ with various values of r_A. The term unbiased refers to critical point and exponent estimates which are determined directly from the approximants, without additional assumptions or information. The estimates quoted are based on averaging all near-diagonal ((n, n) and $(n, n \pm 1)$) non-defective approximants. Here an approximant is defined as defective if there is a real singularity between $-x_c$ and $(1 + \varepsilon_1)x_c$, or if there is a complex conjugate singularity pair at z and z^* with $|\mathrm{Im}(z)| < \varepsilon_2$ with $\varepsilon_1 = 0.2$ and $\varepsilon_2 = 0.005$. When almost all approximants are defective (defined as three or fewer non-defective), all the approximants were used to compute the average. In this case, the quoted exponent value is marked by an asterisk.

The subcritical and supercritical series data show that the two second-order transition points are distinct in the regime $r_A < r_A^t$, but become virtually identical for $r_A > r_A^t$, with $r_A^t \cong 0.45$. For $r_A < r_A^t$, the exponents obtained from analysing both series

Table 2. Estimates of the critical parameters for $\bar{P}(0)$ for the interacting model with $r_B = 1$.

r_A	Lower p_c	Lower $\nu(1-\delta)$	Upper p_c	Upper $\nu(1-\delta)$
0.0	0.5909 ± 0.0005	1.438 ± 0.054		
0.1	0.5853 ± 0.0005	1.447 ± 0.056	0.7682 ± 0.0006	1.483 ± 0.060
0.2	0.5787 ± 0.0006	1.479 ± 0.062	0.6684 ± 0.0007	1.429 ± 0.088
0.3	0.5712 ± 0.0005	1.522 ± 0.052	0.6118 ± 0.0009	1.402 ± 0.092
0.4	0.5621 ± 0.0005	1.503 ± 0.075	0.5783 ± 0.0009	1.193 ± 0.082
0.5	0.5497 ± 0.0011	1.206 ± 0.078	0.5546 ± 0.0008	1.153 ± 0.092
0.6	0.5378 ± 0.0006	1.016 ± 0.038	0.5399 ± 0.0006	0.954 ± 0.037
0.7	0.5276 ± 0.0002	0.928 ± 0.014	0.5279 ± 0.0003	0.851 ± 0.016
0.8	0.5170 ± 0.0003	0.817 ± 0.019	0.5184 ± 0.0004	0.762 ± 0.026
0.9	0.5068 ± 0.0003	0.721 ± 0.020	0.5100 ± 0.0004	0.712 ± 0.029
1.0	0.4975 ± 0.0007	0.671 ± 0.048	0.4975 ± 0.0007	0.671 ± 0.048

Table 3. Estimates of the critical parameters for $\tilde{N}_E(0)$ for the interacting model with $r_B = 1$.

r_A	Lower p_c	Lower $\nu(1+\eta_E)$	Upper p_c	Upper $\nu(1+\eta_E)$
0.0	0.5911 ± 0.0005	2.282 ± 0.053		
0.1	0.5854 ± 0.0003	2.287 ± 0.036	0.7685 ± 0.0004	2.289 ± 0.039
0.2	0.5786 ± 0.0002	2.273 ± 0.0927	0.6685 ± 0.0004	2.247 ± 0.039
0.3	0.5708 ± 0.0002	2.225 ± 0.020	0.6119 ± 0.0006	2.165 ± 0.062
0.4	0.5613 ± 0.0002	2.074 ± 0.018	0.5779 ± 0.0003	1.911 ± 0.027
0.5	0.5507 ± 0.0001	1.843 ± 0.017	0.5545 ± 0.0004	1.730 ± 0.035
0.6	0.5396 ± 0.0002	1.587 ± 0.028	0.5382 ± 0.0002	1.535 ± 0.015
0.7	0.5288 ± 0.0004	1.363 ± 0.049	0.5260 ± 0.0003	1.339 ± 0.042
0.8	0.5190 ± 0.0006	1.248 ± 0.055	0.5163 ± 0.0003	1.182 ± 0.023
0.9	0.5087 ± 0.0002	1.064 ± 0.019	0.5078 ± 0.0003	1.065 ± 0.018
1.0	0.5000 ± 0.0000	1.000 ± 0.000	0.5000 ± 0.0000	1.000 ± 0.000

are consistent with the corresponding values from RFT, with the subcritical series providing better agreement with RFT. When the transition points merge, exponent estimates change substantially as r_A increases beyond r_A^t. This feature had been found to be characteristic of the discontinuous transition in the monomer–dimer model [18]. Thus series analysis suggests that there is a tricritical point at $(p^t, r_A^t) \cong (0.56, 0.45)$ in the interior of the phase diagram. This is in contrast to the mean-field prediction of a tricritical point at the monomer–monomer limit. Analysis of the symmetric case indicates a qualitatively similar topology for the phase diagram, but with the additional feature of the obvious symmetry about $p = \frac{1}{2}$ (figure 1(b)).

More precise estimates of critical exponents can often be obtained if we use independent accurate values for the location of the critical point. We found that the p_c values obtained from time-dependent Monte Carlo simulations (to be described in the next section) are rather more precise than the series estimates. Thus at several points on the phase diagram (marked in figure 1(a)), we used Monte Carlo estimates for p_c as the basis for computing biased approximants for exponents. The results of this approach give exponents which are very close to those of RFT (table 5).

Table 4. Estimates of the critical parameters for $\tilde{N}_T(0)$ for the interacting model with $r_B = 1$. Here, $N_T(t)$ is defined as the total number lattice sites which are not occupied by Bs.

r_A	Lower p_c	Lower $\nu(1+\eta_T)$	Upper p_c	Upper $\nu(1+\eta_T)$
0.0	0.5908 ± 0.0005	2.240 ± 0.062		
0.1	0.5891 ± 0.0012	2.317 ± 0.122	0.7683 ± 0.0003	2.310 ± 0.026
0.2	0.5796 ± 0.0007	2.379 ± 0.096	0.6682 ± 0.0006	2.299 ± 0.055
0.3	0.5715 ± 0.0001	2.375 ± 0.015	0.6108 ± 0.006	2.334 ± 0.073
0.4	0.5619 ± 0.0001	2.228 ± 0.008	0.5773 ± 0.0006	2.118 ± 0.044
0.5	0.5509 ± 0.0001	2.127 ± 0.013	0.5550 ± 0.0002	1.958 ± 0.016
0.6	0.5391 ± 0.0003	1.920 ± 0.022	0.5394 ± 0.0005	1.806 ± 0.053
0.7	0.5278 ± 0.0003	1.755 ± 0.025	0.5279 ± 0.0003	1.672 ± 0.047
0.8	0.5165 ± 0.0003	1.585 ± 0.025	0.5186 ± 0.0003	1.557 ± 0.031
0.9	0.5063 ± 0.0002	1.493 ± 0.021	0.5104 ± 0.0002	1.507 ± 0.024
1.0	0.4984 ± 0.0002	1.689 ± 0.034	0.4984 ± 0.0002	1.689 ± 0.034

Table 5. Biased estimates of critical parameters for the interacting model at specified points in the phase diagram of figure 1. The * indicates that defective approximants were used in determining the numerical estimate for $\nu\delta$. The RFT exponents are taken from [15].

Point	p_c	$\nu\delta$	$\nu(1-\delta)$	$\nu(1+\eta_E)$	$\nu(1+\eta_T)$
a	0.5910	0.281 ± 0.002	1.459 ± 0.027	2.281 ± 0.013	2.285 ± 0.023
b	0.7687	0.291 ± 0.013*	1.447 ± 0.029	2.269 ± 0.011	2.283 ± 0.030
c	0.6111	0.276 ± 0.011	1.477 ± 0.043	2.242 ± 0.036	2.297 ± 0.025
d	0.5709	0.312 ± 0.004	1.506 ± 0.041	2.240 ± 0.009	2.317 ± 0.020
e	0.2324	0.262 ± 0.016	1.458 ± 0.022	2.279 ± 0.034	2.285 ± 0.022
f	0.4004	0.274 ± 0.003	1.439 ± 0.024	2.276 ± 0.008	2.280 ± 0.004
g	0.4714	0.272 ± 0.002*	1.476 ± 0.021	2.278 ± 0.051	2.239 ± 0.015
RFT		0.277 ± 0.001	1.447 ± 0.002	2.281 ± 0.002	

Another interesting feature of the series approaches is that they provide two new exact results at the monomer–monomer limit. By the very simple form of their respective series expansions, we infer that $P_\infty = (2p-1)/p$ and $\tilde{N}_E(0) = 1/(1-2p)$. The first result can be explained by the fact that the dynamics of the quantity $n(t) = (N_A(t) + 2N_E(t))$ is identical to a state-dependent random walk, in which the probabilities of going from state n to $n+1$, $n-1$, and n, are $pW(n)$, $(1-p)W(n)$ and $W(n)$, respectively. Here $W(n)$ is an unknown function of n, but the crucial point is that the ratio of the hopping probabilities do not involve $W(n)$. The initial condition where all sites are occupied by Bs except for a single empty site corresponds to a random walk in n-space which starts one step away from an absorbing boundary at $n=0$. Since the ultimate survival probability depends only on the ratio $(pW(n))/[(1-p)W(n)] = p/(1-p)$, the functional form of P_∞ at $r_A = 1$ is identical to that of a pure random walk which starts one step from an absorbing boundary. We have, however, not yet been able to find a simple explanation for the apparent exact result for $\tilde{N}_E(0)$.

6. Monte Carlo simulations

To check the series results by independent means, we performed Monte Carlo (MC) simulations of the interacting surface reaction model. Our goal was to obtain additional evidence for the existence of a tricritical point in the model. We first performed time-dependent MC simulations at several representative points which lie to the left of the tricritical point (figure 1). This simulation method provides an efficient and accurate method for determining the critical parameters of models that exhibit a continuous phase transition to an absorbing state [1, 19–22]. The reaction is simulated with all the sites initially occupied by a single species (either As or Bs, depending on where in the phase diagram one wishes to examine) except for a single vacancy. During the simulation, we track the number of empty sites, $N_E(t)$, and the number of the species opposite from those in the initial state, $N_o(t)$. The lattice is sufficiently large so that the initial defect cannot reach the boundary throughout the simulation. The simulation was run for up to 2000 time steps and averages over 2.5×10^5 independent runs were performed.

We measured: (i) the survival probability $P(t)$; (ii) the average number of empty sites $N_E(t)$ and the average number of the other species $N_o(t)$; and (iii) the mean-

square spread of the region of empty sites, $R^2(t)$. At the critical point p_c, the scaling assumption discussed in section 4 implies that for large t, these quantities have the following power law time dependences

$$P(t) \sim t^{-\delta} \tag{25}$$

$$N_E(t) \sim t^{\eta_E} \qquad N_o(t) \sim t^{\eta_o} \tag{26}$$

and

$$R^2(t) \sim t^z. \tag{27}$$

Thus at p_c, graphs of $\log P(t)$, $\log N_E(t)$, $\log N_o(t)$, and $\log R^2(t)$ versus $\log t$ should asymptotically fall on a straight line, while off-critical plots will exhibit curvature. More precise estimates for the critical exponents can be obtained by examining the trend in the local slopes of the data, when plotted on a double logarithmic scale. For example, for $P(t)$, we define the effective exponent as

$$-\delta(t) = \frac{\log[P(t)/P(t/b)]}{\log b} \tag{28}$$

where we have chosen $b = 5$ for most of our extrapolations. We then estimate the asymptotic value of the exponent, by using the fact that the pre-asymptotic corrections can be written as [19]

$$\delta(t) = \delta + \frac{a}{t} + \frac{a'}{t^{\delta'}} + \cdots \tag{29}$$

where a, a' and δ' are constants, to monitor how the effective exponent approaches its limiting value as $1/t \to 0$. Similar expressions exist for $\eta_E(t)$, $\eta_o(t)$ and $z(t)$.

Plots of the effective exponent against $1/t$ exhibit either upward or downward curvature in the plots away from criticality. Since the direction of this curvature depends sensitively on the value of p, a relatively accurate estimate for p_c may be deduced. The value of the exponent is then estimated by the intercept of the data on the vertical axis when $p = p_c$. A typical example of such a plot is shown in figure 3, which corresponds to point c in the phase diagram of figure 1(a). Figure 3(c) shows that the local slope $\eta_E(t)$ veers downward (subcritical) for $p = 0.6113$ and upward (supercritical) for $p = 0.6009$. Therefore, our estimate for the critical point is $p_c = 0.6111 \pm 0.0002$ and the corresponding exponent $\eta_E = 0.31 \pm 0.02$. The quoted error bars represent a subjective estimate of the range over which the curvature of the data when plotted against $1/t$ does not indicate a systematic upward or downward trend. Once the critical point is determined, we use this information to estimate the other critical exponents δ, η_B and z from the asymptotic values of the corresponding local slope when plotted against $1/t$. The results of this analysis are summarized in table 6, along with the corresponding exponents values of RFT. Our estimates for the exponents at the representative points of the phase diagram with $r < r_A'$ are in good agreement with those of RFT. Thus, the time-dependent MC simulations corroborate the series results.

However, both the series and the Monte Carlo results do not unambiguously rule out the possibility that a narrow region of steady-state behaviour exists, even as $r_A \to 1$. In fact, the Monte Carlo merely indicated that the critical exponents change continuously along the transition line as r is increased beyond r_c. Such a feature was found to be indicative of a first-order transition in the monomer–dimer model [18].

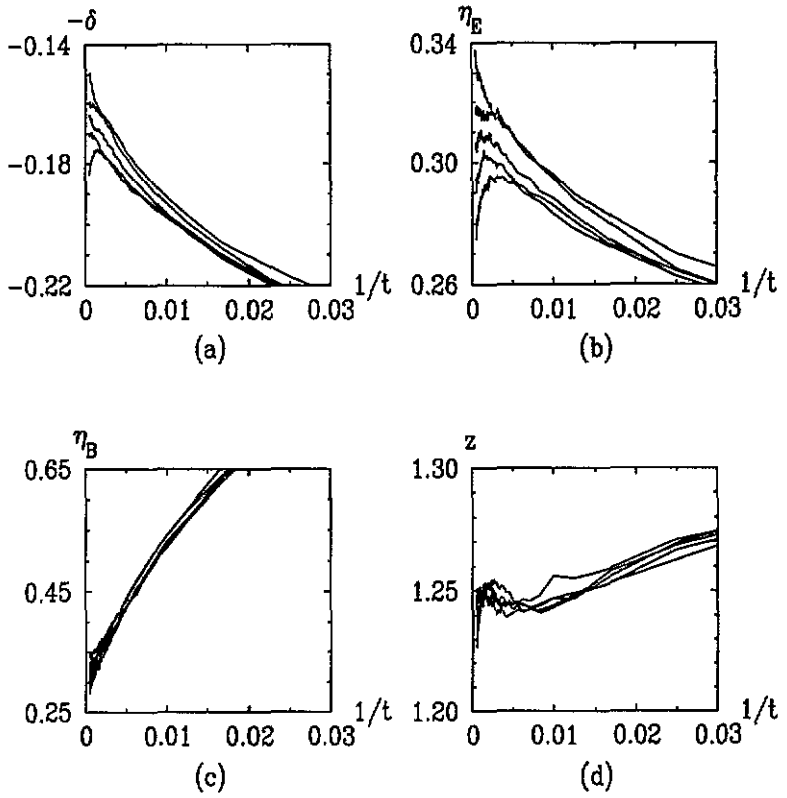

Figure 3. Plots of the effective exponents versus $1/t$ at the point corresponding to the point marked c in figure 1(a). The five curves, from the bottom to top, correspond to $p=0.6115$, 0.6113, 0.6111, 0.6009, and 0.6007.

However, to provide direct evidence for a first-order transition for $r>r_c$, we use a complementary Monte Carlo approach which appears suitable for distinguishing sensitively between a second-order and first-order transition. We follow the time development of the system from a 'kink' initial condition, i.e. a lattice filled with Bs for $x<0$, with As for $x>0$, and with a vacancy at $x=0$. If there is a first-order transition between A- and B-saturated phases at $p=p_c$, then the kink should move to the left for $p>p_c$ and to the right for $p>p_c$, with the kink width growing at a negligible

Table 6. Critical parameter estimates from the time-dependent MC simulation at specified points in the phase diagram of figure 1.

Point	p_c	δ	η_E	η_0	z
a	0.5910 ± 0.0002	0.155 ± 0.010	0.32 ± 0.02	0.33 ± 0.02	1.24 ± 0.02
b	0.7687 ± 0.0002	0.160 ± 0.008	0.31 ± 0.01	0.32 ± 0.01	1.25 ± 0.01
c	0.6111 ± 0.0002	0.165 ± 0.005	0.31 ± 0.02	0.32 ± 0.02	1.25 ± 0.03
d	0.5709 ± 0.0002	0.160 ± 0.010	0.31 ± 0.02	0.33 ± 0.03	1.25 ± 0.03
e	0.2324 ± 0.0002	0.160 ± 0.005	0.31 ± 0.01	0.32 ± 0.01	1.25 ± 0.02
f	0.4004 ± 0.0002	0.160 ± 0.004	0.31 ± 0.01	0.32 ± 0.01	1.26 ± 0.01
g	0.4714 ± 0.0003	0.161 ± 0.010	0.32 ± 0.02	0.32 ± 0.03	1.24 ± 0.03
RFT		0.160 ± 0.003	0.317 ± 0.002		1.272 ± 0.007

rate to the translational motion. This qualitative behaviour is readily observed in simulations of the monomer–monomer model. On the other hand, near a second-order transition to a reactive steady state, the kink width will grow much faster than its translational motion. These qualitative differences in the development of a kink are the criteria we use to infer the character of the phase transition.

For example, for the case where $r_A = 0.7$ and $r_B = 1$, we find the following behaviour, based on 50 000 realizations of up to 2500 time steps. For $p = 0.5273$, the mean position of the kink is systematically moving to the right and has reached 1.79 (in lattice units) at 2500 time steps. The average width of the kink equals the fixed value of 7.84 by this time. However, for $p = 0.5275$ the mean position of the kink has moved -1.79 to the left while maintaining a fixed width of 7.82. These results suggest the existence of a first-order transition for $p \cong 0.527\,40$. On the other hand, for $r_A = 0.3$, there is definite translational kink motion for $p \leqslant 1$, while the kink merely grows in width without translating for $p < p_c$. This behaviour is indicative of a second-order phase transition from A-saturation to a steady state.

A complementary approach was taken for the symmetric model where $r_A = r_B \equiv r$. In this case we fix p to be somewhat larger than 0.5, and examine the evolution of a kink as a function of r. The existence of a tricritical point would imply that the A-saturated phase would be stable for a finite range of r between a critical value and unity (figure 1(b)). For example, for $p = 0.51$ we find that the region of A-saturation extends to at least $r \cong 0.7$, based on the range of values of which a kink translates with negligible spreading. When $p = 0.502$, this region of A-saturation extends to least $r \cong 0.8$. The net conclusion from the two data sets is that a first-order line extends a finite distance from the monomer–monomer limit. These kink evolution studies provides indirect, yet relatively strong evidence for the existence of a tricritical point.

7. Summary and discussion

We have investigated the role of adsorbate interactions on a simple model of surface reactions in which there is a variable repulsive interaction between same species reactants. The special cases of an excluded-volume interaction among only one species, and a symmetric system with the same excluded-volume interaction for both species have been considered. For strong repulsion, this system exhibits two continuous RFT-type transitions between a reactive steady state, and A- and B-saturated states as a function of the relative deposition rates of the two species. For weak repulsion, there is only a single first-order transition between A- and B-saturated states as a function of relative deposition rates. Using series expansions and Monte Carlo simulation approaches, we mapped out the phase diagram of the system and estimated the critical parameters of the associated non-equilibrium phase transitions. The numerical data suggests the existence of a tricritical point at the confluence of the first- and second-order transitions which is located at a non-zero value of the interaction strength.

Within the stoichiometry of the monomer–monomer model, it would be interesting to examine the effects of other basic microscopic features that can occur in realistic adsorption processes. Typical examples include attractive interactions between adsorbates [10] and various non-linear adsorption processes [23]. By such studies, one may be able to gain new insights about how the details of the elemental steps of surface reactions affect the macroscopic kinetic features, such as the universality classes of the

non-equilibrium phase transitions that result. A repulsive interaction may also give rise to anomalous effect in the monomer–dimer model. For example, if the monomers experience a particular type of excluded-volume repulsion in which a monomer cannot adsorb on vacancies in which all nearest neighbours are occupied by monomers, then an infinitely degenerate monomer-only phase occurs. Consequently, an unusual non-equilibrium phase transition may arise between this degenerate state and a reactive phase.

It would also be desirable to have better numerical tools to probe of the nature of the phase diagram more definitively. Although the series method is appropriate for studying second-order non-equilibrium phase transitions, this method indicates that certain physical quantities exhibit power law behaviour with non-universal exponents at a first-order transition. There is not yet a clear physical interpretation of these results. It would also be worthwhile to find the underlying basis for the power law behaviour of P_∞ and $\tilde{N}_E(0)$ at the first-order transition in the monomer–monomer model.

Acknowledgments

We thank R Dickman and I Jensen for helpful discussions and A J Guttmann for sending us his program for computing differential approximants. Acknowledgement is made to the Donors of the Petroleum Research Fund, administered by the American Chemical Society, for partial support of this research. This work is also supported in part by a grant from the ARO.

References

[1] Grassberger P 1982 *Z. Phys.* B **47** 365
[2] Janssen H K 1981 *Z. Phys.* B **42** 151
[3] Dickman P and Burschka M 1988 *Phys. Lett.* **127A** 132
[4] Grinstein G, Lai Z-W and Browne D A 1989 *Phys. Rev.* A **40** 4820
[5] Ziff R M, Gulari E and Barshad Y 1986 *Phys. Rev. Lett.* **56** 2553
[6] Meakin P and Scalapino D J 1987 *J. Chem. Phys.* **87** 731
[7] Dickman R 1986 *Phys. Rev.* A **34** 4246
[8] Fischer P and Titulaer U M 1989 *Surf. Sci.* **221** 409
[9] Takoudis C G, Schmidt L D and Aris R 1981 *Surf. Sci.* **105** 325
[10] Kaukonen H-P and Nieminen R M 1989 *J. Chem. Phys.* **91** 4380
[11] Schick M 1982 *Prog. Surf. Sci.* **11** 245; 1982 *Physica* **110** 1811
[12] Park H, Köhler J, Kim I-M, ben-Avraham D and Redner S 1993 *J. Phys. A: Math. Gen.* **26** 2071
[13] Ziff R M and Fichthorn K 1986 *Phys. Rev.* B **34** 2038
ben-Avraham D, Considine D, Meakin P, Redner S and Takayasu H 1990 *J. Phys. A: Math. Gen.* **23** 4297
[14] Grassberger P and de la Torre A 1979 *Adv. Phys.* **122** 373
[15] Dickman R and Jensen I 1991 *Phys. Rev. Lett.* **67** 2391
[16] Jensen I and Dickman R 1993 *J. Stat. Phys.* **71** 89
[17] Guttmann A J 1989 in *Phase Transition and Critical Phenomena* **13** ed C Domb and J Lebowitz (New York: Academic)
[18] Evans J W and Miesch M S 1991 *Phys. Rev. Lett.* **66** 833
[19] Grassberger P 1989 *J. Phys. A: Math. Gen.* **22** 2673
[20] Dickman R 1989 *Phys. Rev.* B **40** 7005
[21] Dickman R 1990 *Phys. Rev.* A **42** 6985
[22] Jensen I, Fogedby H C and Dickman R 1990 *Phys. Rev.* A **41** 3411
Jensen I 1991 *Phys. Rev.* A **43** 3187; *Phys. Rev.* A **45** 563
[23] Horgan A M and King D A 1972 *Adsorption-Desorption Phenomena* (New York: Academic)